952–961 *Nucleic Acids Research, 2022, Vol. 50, No. 2* *Published online 30 December 2021*
https://doi.org/10.1093/nar/gkab1270

Structure–activity relationships at a nucleobase-stacking tryptophan required for chemomechanical coupling in the DNA resecting motor-nuclease AdnAB

Garrett M. Warren [1], Aviv Meir[2], Juncheng Wang[3], Dinshaw J. Patel[3], Eric C. Greene[2] and Stewart Shuman [1,*]

[1]Molecular Biology Program, Sloan Kettering Institute, New York, NY 10065, USA, [2]Department of Biochemistry and Molecular Biophysics, Columbia University, New York, NY 10032, USA and [3]Structural Biology Program, Sloan Kettering Institute, New York, NY 10065, USA

Received October 27, 2021; Revised December 07, 2021; Editorial Decision December 12, 2021; Accepted December 13, 2021

ABSTRACT

Mycobacterial AdnAB is a heterodimeric helicase-nuclease that initiates homologous recombination by resecting DNA double-strand breaks. The AdnB subunit hydrolyzes ATP to drive single-nucleotide steps of 3′-to-5′ translocation of AdnAB on the tracking DNA strand via a ratchet-like mechanism. Trp325 in AdnB motif III, which intercalates into the tracking strand and makes a π stack on a nucleobase 5′ of a flipped-out nucleoside, is the putative ratchet pawl without which ATP hydrolysis is mechanically futile. Here, we report that AdnAB mutants wherein Trp325 was replaced with phenylalanine, tyrosine, histidine, leucine, or alanine retained activity in ssDNA-dependent ATP hydrolysis but displayed a gradient of effects on DSB resection. The resection velocities of Phe325 and Tyr325 mutants were 90% and 85% of the wild-type AdnAB velocity. His325 slowed resection rate to 3% of wild-type and Leu325 and Ala325 abolished DNA resection. A cryo-EM structure of the DNA-bound Ala325 mutant revealed that the AdnB motif III peptide was disordered and the erstwhile flipped out tracking strand nucleobase reverted to a continuous base-stacked arrangement with its neighbors. We conclude that π stacking of Trp325 on a DNA nucleobase triggers and stabilizes the flipped-out conformation of the neighboring nucleoside that underlies formation of a ratchet pawl.

INTRODUCTION

Mycobacterial AdnAB is a heterodimeric ATP-dependent helicase-nuclease that initiates homologous recombination by resecting DNA double-strand breaks (DSBs) (1–3). The AdnA and AdnB subunits are encoded in a two-gene operon that is transcriptionally upregulated in response to DNA damage (4–6). AdnA and AdnB are paralogs composed of an N-terminal ATP-binding motor or motor-like domain and a C-terminal nuclease domain. The working model for DSB resection by AdnAB—based on ensemble and single-molecule biochemistry, mutagenesis, atomic force microscopy, and cryo-electron microscopy (1,7–11)—posits that: (i) initial ATP-independent binding of AdnAB to a DSB end melts a short segment of the duplex to allow access of the 5′ terminal strand to the AdnA nuclease active site and access of the 3′ terminal strand to the AdnB motor; (ii) ATP hydrolysis catalyzed by the AdnB motor then drives translocation of tandem AdnB motor and AdnA motor-like domains in the 3′ to 5′ direction along the tracking strand, with the AdnB motor domain in the lead; (iii) translocation propels the 3′ tracking strand along a sequential path through the AdnB motor and AdnA motor-like domains and then into the AdnB nuclease domain; and (iv) ATPase-coupled DNA unwinding simultaneously threads the 5′ DNA strand through the AdnA nuclease domain (Supplementary Figure S1). Once engaged, the AdnAB motor-nuclease resects duplex DNA rapidly (∼450 bp/s on average in single-molecule assays) and processively (∼37 kb average resection tract length) (10). Because the average rate of DSB resection is similar to the apparent k_{cat} of 415 s^{-1} for ssDNA-dependent ATP hydrolysis, it is surmised that 1 bp is unwound by AdnAB per ATP hydrolyzed. AdnAB is prone to spontaneous pausing at random sites during the resection of long dsDNA substrates; a notable property of AdnAB is that the velocity of DSB resection slows after the enzyme experiences a spontaneous pause (10,11). Outstanding mechanistic issues concern the physical basis for the chemomechanical coupling of ATP hydrolysis to DNA unwinding.

*To whom correspondence should be addressed. Tel: +1 212 639 7145; Email: s-shuman@ski.mskcc.org

Insights ensued from a set of cryo-EM structures of DNA-free AdnAB and AdnAB bound to a duplex DNA with 5′ and 3′ tails, which revealed: (i) the path of the unwound 5′ strand and its contacts with the AdnA nuclease; (ii) the path of the 3′ tracking strand through the AdnB motor; and (iii) an AdnA iron-sulfur cluster subdomain at the Y-junction that maintains the split trajectories of the unwound 5′ and 3′ strands (10). The AdnB–ssDNA interface entails a network of amino acid side chain contacts to the phosphates and nucleobases of a 7- to 8-nucleotide 3′ ssDNA tail. Trp325, Arg326, Phe254, and Leu142 stack on and between the nucleobases, acting as baffles to partition the 3′ ssDNA into discrete base-stacked segments (Figure 1A and Supplementary Figure S2). The register of the stacked nucleobase segments was shifted by a one-nucleotide step in two different cryo-EM structures of AdnAB, suggesting that a similar shift occurs during the mechanical power stroke, whereby protein subdomain movements within the AdnB motor, synchronized to the ATP hydrolytic cycle, drive passage of the nucleobases over the amino acid baffles in the 3′ to 5′ direction, and the baffles prevent backward sliding in a pawl-and-ratchet-like fashion (10).

The cryo-EM structures guided a comprehensive alanine scan of the 16 amino acids at the AdnB-DNA interface aimed at discerning which DNA contacts are necessary to couple ATP hydrolysis to motor activity (11). Mutant AdnAB enzymes were assayed for DNA-dependent ATP hydrolysis, DNA translocation, and DSB resection in ensemble and single-molecule formats. The results pinpointed the AdnB amino acid Trp325 (a constituent of SF1 helicase motif III) as the singular essential constituent of the putative ratchet pawl, insofar as: (i) W325A mutant AdnAB was inert in ATP-dependent DSB resection; (ii) W325A AdnAB was defective for ATP-dependent translocation on ssDNA; (iii) W325A AdnAB had the same specific activity in ssDNA-dependent ATP hydrolysis as wild-type AdnAB; and (iv) W325A and wild-type AdnAB had similar apparent K_m values for the ssDNA activator of ATP hydrolysis (236 and 192 nM, respectively), i.e. loss of the tryptophan did not impede ssDNA binding (11).

The essential Trp325 makes a π stack on a nucleobase 5′ of a nucleoside that is flipped out between base-stacked segments of the tracking strand (Figure 1A and Supplementary Figure S2). Its neighbor Arg326, which makes a cation–π stack on the nucleobase 3′ of the flipped-out nucleoside (Figure 1A and Supplementary Figure S2), is not essential for ATP hydrolysis or DNA resection (11). Leu142 and Phe254, which intercalate into the tracking strand further downstream (Figure 1A and Supplementary Figure S2), also proved not to be important for AdnAB motor activity (11). Of the 16 amino acids that comprise the AdnB–DNA interface, only three beside Trp325 were important for chemomechanical coupling: Thr118, Thr663, and His665 (Figure 1A). The T118A, T663A, and H665A mutants retained vigorous ssDNA-dependent ATPase activity but displayed feeble DSB resection activity in ensemble assays and resected DNA with drastically reduced velocity *vis-à-vis* wild-type AdnAB in single-molecule assays (11). It was surmised that loss of Thr118, Thr663, and His665 contacts to the tracking strand lowers the microscopic efficiency of the AdnB motor, such that a significant fraction of the ATP hydrolytic events is unproductive with respect to translocation, resulting a monotonously slow motor.

In its role as the uniquely essential strand-intercalating ratchet pawl, Trp325 could disfavor backsliding of AdnAB in either of two ways: via the stabilizing effect of its π stack over the nucleobase; by promoting the flipping of the adjacent nucleoside; or a combination of both effects. To address the issue of π stacking, we characterize herein the effects of conservative substitutions for AdnB Trp325 in which the tryptophan is replaced by other aromatic amino acids (phenylalanine, tyrosine, histidine) or by a gamma-branched aliphatic amino acid (leucine). We find that whereas all the mutants were active in ssDNA-dependent ATP hydrolysis, the phenylalanine and tyrosine variants retained DNA resection activity, while the His mutant was severely defective, and the leucine mutant was inert *à la* alanine. A cryo-EM structure of the W325A AdnAB mutant bound to tailed duplex DNA revealed that the AdnB peptide segment comprising mutated motif III was disordered and the erstwhile flipped out nucleobase reverted to a continuous base-stacked arrangement with its neighbors. We surmise that π stacking of motif III Trp325 over a tracking strand nucleobase elicits and stabilizes a flipped-out conformation that is necessary to create a ratchet pawl.

MATERIALS AND METHODS

Recombinant AdnAB proteins

Wild-type and mutant AdnAB heterodimers were produced in *E. coli* by co-expression of His_{10}Smt3-tagged AdnA and un-tagged AdnB subunits and purified from soluble extracts by sequential nickel-agarose affinity chromatography, cleavage of the His_{10}Smt3 tag by treatment with the Smt3-specific protease Ulp1, separation of tag-free AdnAB from His_{10}Smt3 by passage over a second nickel-agarose column, and a final Superdex-200 gel filtration step (1,10). The protein concentrations were determined by using the BioRad dye reagent with BSA as the standard.

Single molecule DNA curtain assays

All experiments were performed with a custom-built prism-type total internal reflection fluorescence (TIRF) microscope (Nikon) equipped with a 488-nm laser (Coherent Sapphire, 200 mW) and two Andor iXon EMCCD cameras (12). Flowcells and single-tethered dsDNA curtains were prepared as described previously (13) using bacteriophage λ DNA (48.5 kb; NEB Cat No. N3011S) that was biotinylated at one end and anchored to a lipid bilayer through a biotin-streptavidin linkage. All single molecule experiments were performed at 37°C in resection buffer (20 mM Tris–HCl, pH 8.0, 1 mM DTT, 2 mM $MgCl_2$, 0.1 mM ATP, 0.2 mg/ml BSA). DNA was aligned along chromium barriers under a constant buffer flow at 0.15 ml/min and stained with 0.1 mM YOYO-1 for 1 min. Free YOYO-1 was flushed out of the flow cell at 0.5 ml/min for 2 min. End resection was then initiated by the injection of 5 nM AdnAB through

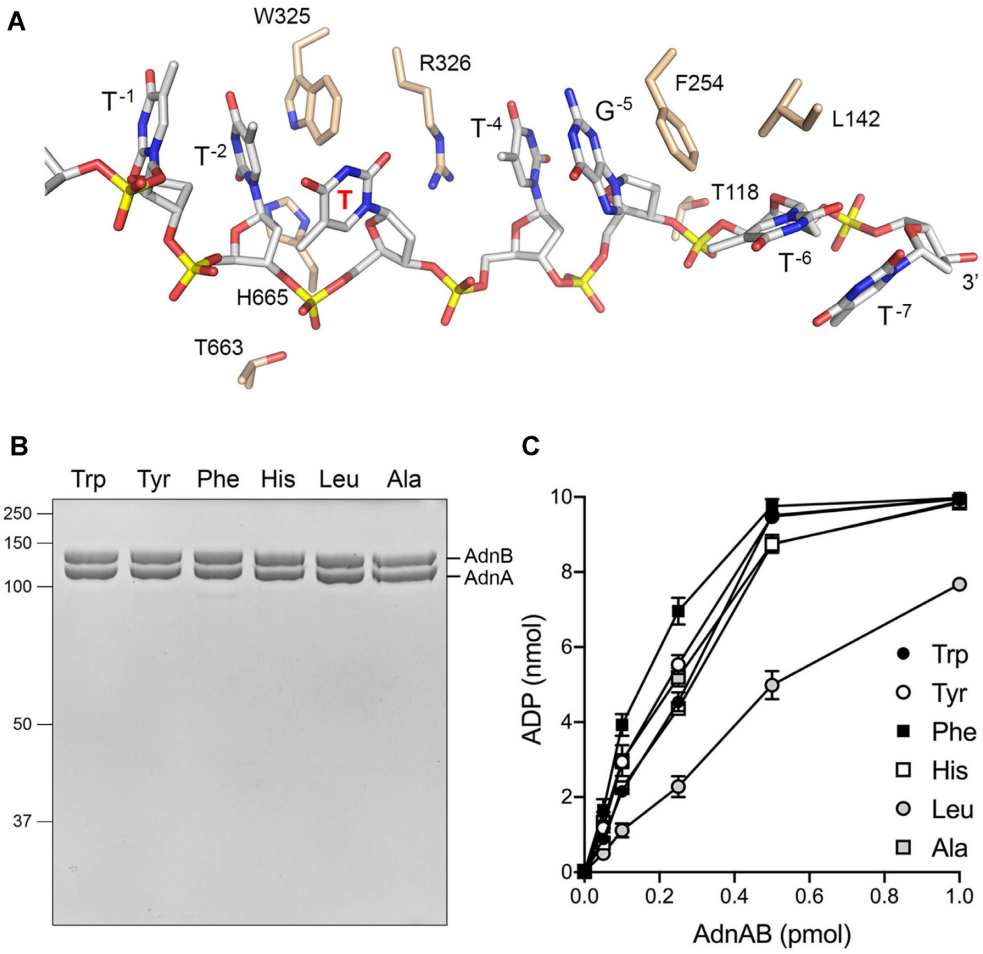

Figure 1. Effects of Trp325 mutations on DNA-dependent ATPase activity. (**A**) A view of the cryo-EM structure of wild-type AdnAB heterodimer bound to forked duplex DNA highlighting the 3′ tracking strand ssDNA interface with selected protein side chains of the AdnB subunit. DNA is depicted as a stick model with gray carbons and yellow phosphorus atoms; the identities of the nucleobases are indicated and numbered by position relative to the duplex junction. The flipped-out thymine (T^{-3}) is indicated in bold red font. Amino acids are rendered as stick models with beige carbons. Trp325, Arg326, Phe254, and Leu142 stack on and between the nucleobases, so as to partition the 3′ ssDNA tracking strand into base-stacked segments: $T^{-1}pT^{-2}$; $T^{-4}pG^{-5}$; and $T^{-6}pT^{-7}$. (**B**) Aliquots (5 μg) of recombinant wild-type AdnAB (with Trp at AdnB position 325) and the indicated mutant heterodimers (with Tyr, Phe, His, Leu, or Ala at position 325) were analyzed by SDS-PAGE. The Coomassie blue-stained gel is shown. The positions and sizes (kDa) of marker polypeptides are indicated on the left. The AdnB and AdnA polypeptides are indicated on the right. (**C**) ATPase reaction mixtures (10 μl) containing 20 mM Tris–HCl (pH 8.0), 2 mM $MgCl_2$, 1 mM DTT, 1 mM (10 nmol) [α^{32}P]ATP, 5 μM 44-mer ssDNA oligonucleotide, and AdnAB as specified were incubated for 10 min at 37°C. The reactions were quenched by adding 2 μl of 5 M formic acid. Aliquots (2 μl) of the mixtures were applied to PEI-cellulose TLC plates, which were developed with 0.45 M ammonium sulfate. [α-^{32}P]ATP and [α-^{32}P]ADP were quantified by scanning the plates with a Typhoon FLA 7000 imager and processing the data with ImageQuant software. The extent of ATP hydrolysis is plotted as a function of input AdnAB. Each datum in the graph is the average of three independent titration experiments ± SEM.

a 150 μl sample loop at 0.15 ml/min and unbound AdnAB was flushed from the sample chamber. End resection was then visualized by the gradual reduction of the length of the fluorescently stained DNA molecules (10). Image acquisition was initiated immediately prior to the protein injections and continued for the durations of the resection assays, which were 5 min for the Trp, Phe, and Tyr AdnAB proteins but were 20 min for the His mutant. Images for the Trp, Phe, Tyr, and Leu AdnAB proteins were acquired at 1 frame per 2 s with 0.1 s integration time, and the illumination laser was shuttered between each image to minimize photo-bleaching. The images for the His mutant were acquired at 1 frame per 10 s.

Optical microscopy image processing and data analysis

Raw TIFF images were imported as image stacks to ImageJ. Images were corrected for drift using the StackReg function in ImageJ. Kymographs were then generated from the corrected image stacks by defining a 1-pixel wide region of interest (ROI) encompassing individual dsDNA molecules and these kymographs were used for analysis of AdnAB resection tract length and velocity as described (13). AdnAB end resection events from the kymographs were fitted with a linear function to calculate AdnAB translocation velocity for each individual molecule. AdnAB translocation velocities were then obtained from Gaussian fits of the distributions of observed velocities.

Preparation of AdnA-AdnB(W325A)-DNA complexes

The DNA ligand (10) was a 70-mer synthetic oligonucleotide designed to form a forked duplex structure comprising a 19-bp duplex with a 5-nucleotide hairpin on one end and a 6-nucleotide 5′ tail and a 21-nucleotide 3′ tail on the other end. A mixture of 15 μM AdnA-AdnB(W325A), 50 μM forked DNA, 1 mM AMPPNP, and 4 mM $MgCl_2$ in 20 mM Tris–HCl (pH 8.0), 150 mM NaCl, 10% glycerol was incubated for 45 min on ice. The sample was filtered through a 0.2 μm spin-filter (Corning) and then gel-filtered through a Superdex-200 column equilibrated in 20 mM Tris, pH 8.0, 150 mM NaCl. The AdnAB peak fraction determined by SDS-PAGE was used to prepare EM grids.

Cryo-EM sample preparation and data acquisition

Aliquots (3.5 μl) of a 0.6 mg/ml solution of gel-filtered AdnA-AdnB(W325A)-DNA complexes were applied to UltrAuFoil 300 mesh R1.2/R1.3 grids (Quantifoil), which were glow-discharged for 120 s at 0.37 mBar, 15 mA in a Pelco easiGlow glow discharge cleaning system (TED PELLA). Grids were blotted for 1.5 s with 100% humidity at 4°C and flash frozen in liquid ethane using a Vitrobot Mark IV (FEI). Images were collected on a 300 keV Titan Krios electron microscope (FEI) with Gatan K3 Summit detector at Memorial Sloan Kettering Cancer Center's Richard Rifkind Center for cryo-EM. The defocus range was set from −1.0 to −2.5 μm. Micrographs were collected in super-resolution mode at an electron dose rate of 20 e^-/pixel/s with a total exposure time of 3 s and intermediate frames were recorded every 0.075 s for a total of 40 frames.

Cryo-EM image processing

The movie frames were motion corrected and 2× Fourier-cropped from a super-resolution pixel size of 0.532 Å using MotionCor2 (14). Contrast transfer function parameters were estimated by CTFFIND-4 (15). Other steps of cryo-EM data processing were performed by RELION-3 (16). 1,710,628 particles were auto-picked with a 2D reference generated in (10) from 2,204 images and extracted at a 3-fold binned pixel size of 3.192 Å. After two rounds of reference-free 2D classification, 483,789 particles were selected for 3D classification using the map of EMD-20447 (10) as an initial reference. 98,408 particles from the best classes were refined, re-extracted to pixel size 1.064 Å and used for 3D refinement along with CTF refinement and particle polishing. The final reconstruction yielded an electron microscopy map of AdnA-AdnB(W325A)-DNA-AMPPNP with a resolution of 3.8 Å. The resolution was estimated using RELION post-processing by applying a soft mask around the protein density and the Fourier shell correlation (FSC) = 0.143 criterion (17). The local resolution was calculated with RELION-3.

Model building and refinement

The atomic model of the AdnA-AdnB(W325A)-DNA-AMPPNP complex was built by docking the structure of the AdnAB-DNA-AMPPNP complex (PDB 6PPU) into the cryo-EM maps using UCSF Chimera (18,19) and then rebuilt and confirmed in Coot (20) based on the bulky amino acid side chains in the primary protein sequence. The model was refined by real-space refinement in Phenix (21) by applying geometric and secondary structure restraints.

RESULTS

Effect of replacing AdnB Trp325 with Phe, Tyr, His, and Leu

Wild-type or mutant AdnAB heterodimers in which amino acid 325 of AdnB was Trp, Phe, Tyr, His, or Leu were produced in *E. coli* and purified from soluble bacterial extracts, yielding 1:1 complexes of AdnB (1095-aa) and AdnA (1045-aa) polypeptides in each case (Figure 1B). The Trp325Ala mutant AdnAB was purified in parallel to serve as an ATPase-active resection-defective control. Enzyme titrations showed that the specific activities of the Phe, Tyr, His, and Ala mutants in ssDNA-dependent ATP hydrolysis were similar to that of wild-type AdnAB (Figure 1C). The specific activity of the Leu mutant was half that of wild-type Trp325 AdnAB (Figure 1C).

Assays of the AdnAB enzymes for their ability to catalyze ATP-dependent resection of linear duplex pUC19 plasmid DNA revealed that the Trp and Phe proteins digested the majority of input plasmid in 0.5 min, whereas the Leu and Ala proteins elicited no apparent DNA resection during a 5 min reaction (Figure 2). The Tyr substitution had a slight effect on the rate of DSB resection, whereby there was a significant population of intact and partially resected plasmids visible at the 0.5 min time point, though the DNA was extensively resected by 1 min and thereafter (Figure 2). This pattern is suggestive of a lag in the initiation step of resection (11). The His mutant was extremely sluggish at DSB resection, i.e. there was minimal DNA shortening after 5 min, whereby most of the DNA migrated just slightly faster than the input substrate (e.g. compare the His 5 min lane to the adjacent Leu 0.5 min lane) and there was a scant diffuse smear of shorter DNA migrating ahead of that (Figure 2).

Single-molecule DNA curtain analysis of DSB resection velocity by Trp235 mutants

The DNA curtain consists of a parallel array of bacteriophage lambda dsDNA molecules tethered at one end to a lipid bilayer surface and aligned along a chrome barrier oriented perpendicular to the direction of liquid flow (22,23). The DNAs are stained with the fluorescent dye YOYO-1 and visualized by total internal reflection fluorescence microscopy. Engagement of the free DNA ends by AdnAB in the presence of ATP and magnesium results in a time-dependent shortening of the fluorescent linear DNAs (10,11). DNA shortening is taken to be synonymous with helicase unwinding and concomitant DSB resection. Here we conducted DNA curtain resection assays for the wild-type and various Trp325 mutants of AdnAB in the presence of 100 μM ATP. The Leu mutant that was inert in pUC19 DNA resection in the ensemble assay format was also incapable of resecting lambda DNA in the curtain assay (just like the Ala mutant). The distributions of velocities of lambda DNA shortening by wild-type AdnAB and other mutants during individual resection tracts are shown

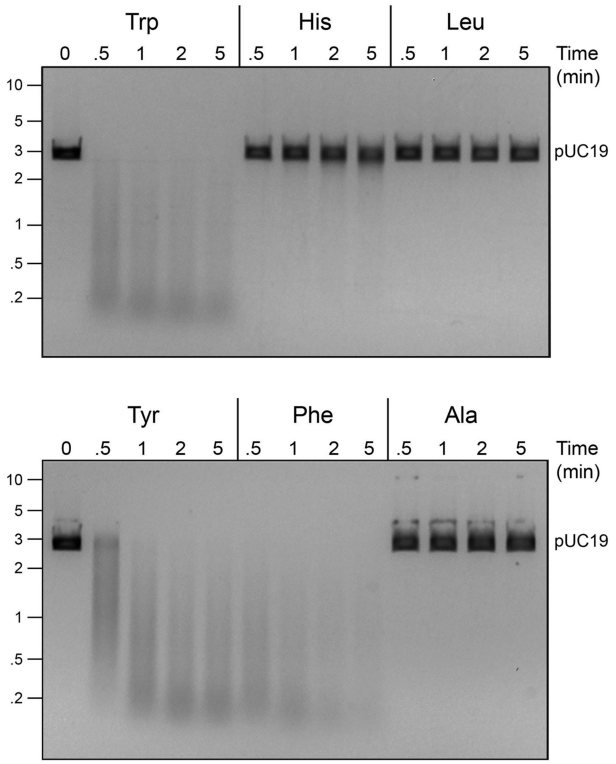

Figure 2. Effects of Trp325 mutations on DNA resection. DSB resection reaction mixtures (60 μl) containing 20 mM Tris–HCl (pH 8.0), 2 mM $MgCl_2$, 1 mM ATP, 1.2 μg linear pUC19 DNA (cut with SmaI), and 15 pmol of wild type or mutant AdnAB were incubated at 37°C. Aliquots (10 μl) were withdrawn at the times specified and the reactions were quenched immediately by adding 2.5 μl of 500 mM EDTA (pH 8.0). The reactions were supplemented with 5 μl of a solution containing 10 mM Tris-HCl (pH 7.6), 60% glycerol, 60 mM EDTA and 0.15% orange G and then analyzed by electrophoresis through a horizontal 0.8% agarose gel containing 0.5x TBE (45 mM Tris-borate, 1.2 mM EDTA). DNA was visualized under shortwave UV illumination after soaking the gel in 0.5× TBE containing 0.5 μg/ml ethidium bromide. The positions and sizes (kb) of linear duplex DNA markers are indicated on the left.

in Figures 3 and 4A. The data were plotted as histograms and fit to Gaussian distributions (red curves) in Figure 3. Scatter plots of the velocities are shown in Figure 4A. For each AdnAB protein in Figures 3 and 4A, we plotted separately: (i) the distribution of velocities at which AdnAB resects from the free end of the phage DNA; and (ii) for those events entailing pausing and resumption of resection after a transient pause, the velocity of movement after a pause. As noted previously (10,11), the rate of wild-type AdnAB resection determined from the Gaussian fits was slower after a pause (368 ± 78 bp/s) than before a pause or in the absence of a pause (433 ± 58 bp/s) (Figure 3A). This decrease was also evident, and statistically significant, in the scatter plots of individual resection events (Figure 4A). Focusing on the initial resection tracts (prior to pausing), we found that the Phe and Tyr mutants resected with reduced velocities, 391 ± 76 bp/s and 367 ± 62 bp/s, respectively (Figure 3B,C), i.e. 90% and 85% of the Gaussian mean value of wild-type AdnAB. These reductions in velocity versus wild-type were statistically significant (Figure 4A). The Phe and Tyr mutants maintained the pattern of statistically significant post-pause slowing of the motor observed for wild-type AdnAB (Figures 3 and 4A). An instructive finding was that the His mutation resulted in a 97% reduction in initial resection velocity (to 12 ± 8 bp/s) *vis-à-vis* wild-type AdnAB, which accounts for the severe kinetic defect seen for the His mutant in the ensemble pUC19 resection assays.

Effects on DSB resection tract length

The DNA curtain reaction endpoint, at which no further DNA shortening is observed, is presumed to reflect dissociation of AdnAB from the DNA substrate. The lengths (in kbp) of individual DNAs that were resected at the endpoint by wild-type and mutant AdnAB enzymes are plotted in Figure 4B. The mean length of DNA resected by wild-type AdnAB was 39.3 ± 9.1 kb. The resection-competent Phe and Tyr mutants had resection track lengths of 33.3 ± 9.6 kbp (*P* value of 0.0002) and 38.4 ± 8.2 kb (not significant), respectively (Figure 4B). By contrast, the tract lengths of the resection-defective His mutant during an extended 20 min observation period were curtailed significantly (2.8 ± 2.3 kb) (Figure 4B). For events entailing a pause and resumption of DNA resection, the distributions of individual pause durations are plotted in Figure 4C. There was no statistically significant difference between the wild-type pause durations (17.5 ± 6.0 s) and those of the Phe mutant (15.1 ± 5.7 s) and the Tyr mutant (15.1 ± 5.7 s).

Cryo-EM structure of W325A mutant AdnAB bound to tailed duplex DNA

AdnA-AdnB(W325A) was preincubated with a forked DNA substrate (comprising a 19-bp duplex with a 5-nucleotide hairpin on one end and a 6-nucleotide 5′ tail and a 21-nucleotide 3′ tail on the other end) in the presence of 1 mM AMPPNP and 4 mM magnesium. The mixture was subjected to gel filtration and the peak AdnAB fraction was applied to grids for cryo-EM analysis as described previously (10). A set of 98,408 particles (20.3% of total 3D class) (Supplementary Figure S3) was used to generate a model of the DNA-bound AdnA-AdnB(W325A) heterodimer at an overall resolution of 3.8 Å (Table S1). The structure is shown in stereo in Figure 5A with the protein subunits depicted as semi-transparent cartoon models and the DNA as a stick model with a cartoon trace through the phosphodiester backbone. AMPPNP was present in the AdnA motor domain (just as it was in the DNA-free AdnAB heterodimer [Supplementary Figure S1B] and wild-type AdnAB•DNA complex [10]), but not in the AdnB motor domain. As noted previously (10), the AdnB nuclease domain was not visible in DNA-bound complexes. The portion of the input forked DNA that was modeled comprised the 13-bp duplex segment at the junction from which a 2-nucleotide 5′ tail and a 7-nucleotide 3′ tail emanate. The duplex DNA segment visualized in the present structure was 3-bp longer than that observed previously (10) and we were able presently to model a previously disordered AdnB segment ^{214}RDR^{216} that penetrates into the minor groove approximately one helical turn upstream of the ds-ss DNA junction. The 5′ ssDNA tail within the AdnA nuclease domain was two nucleotides shorter than the tail seen in the DNA-bound

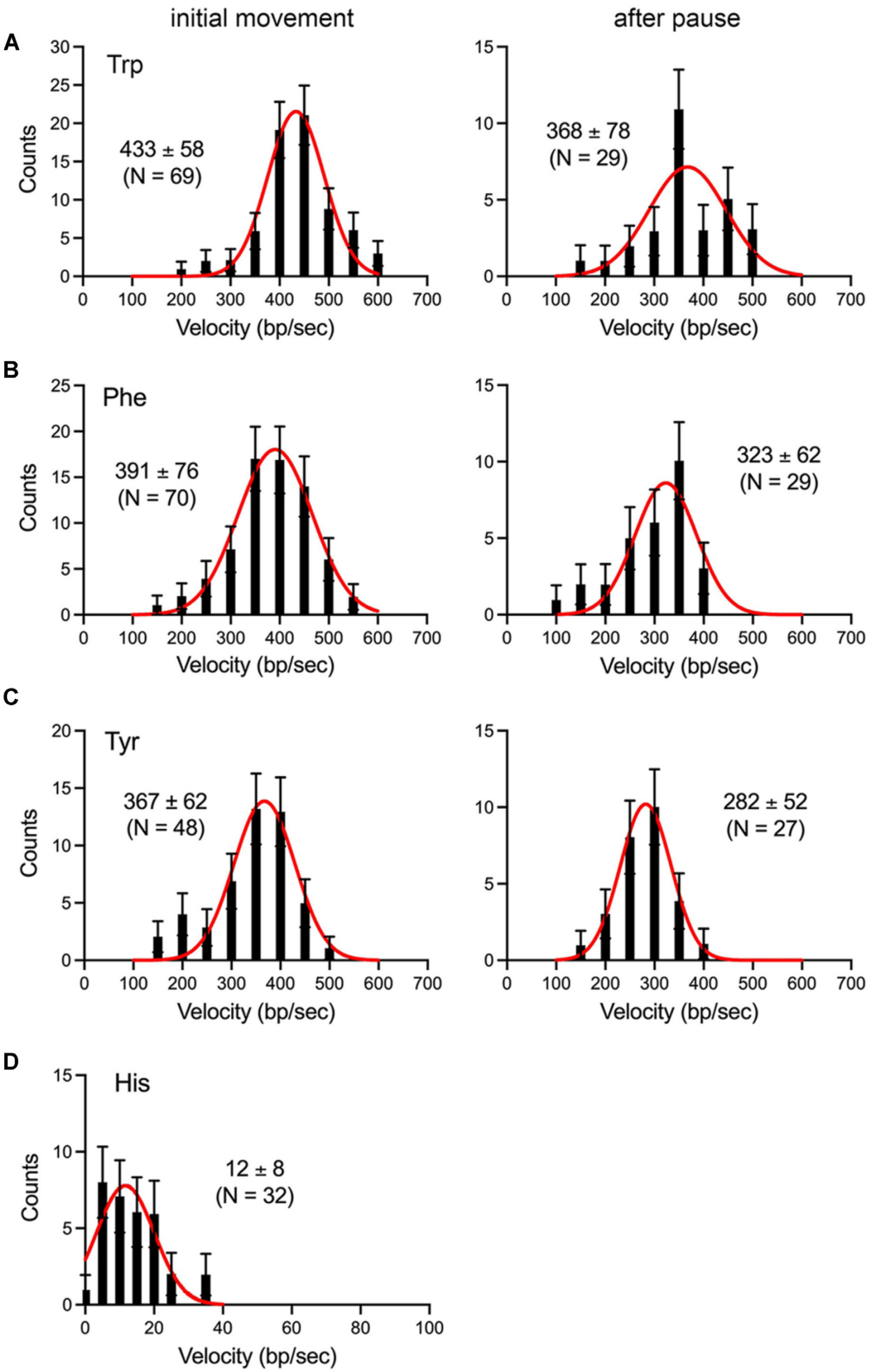

Figure 3. Single-molecule DNA curtain analysis of DSB resection velocity by Trp325 mutants. Velocity distributions of individual resection tracts are shown for wild-type Trp325 AdnAB (panel **A**) and the Phe, Tyr, and His mutants (panels **B**–**D**). For each AdnAB protein, we plotted separately the distribution of velocities at which AdnAB resected from the original end of the phage DNA (initial movement, graphs at left in each panel) and, for those events entailing pausing and resumption of resection after a transient pause, the velocity of movement after a pause (graph at right in each panel). Black error bars represent 95% confidence intervals calculated from bootstrap analysis. The solid red lines represent Gaussian fits to the data. The number of events scored (*N*) and mean velocities (±SD) derived from the Gaussian fit are shown in each graph.

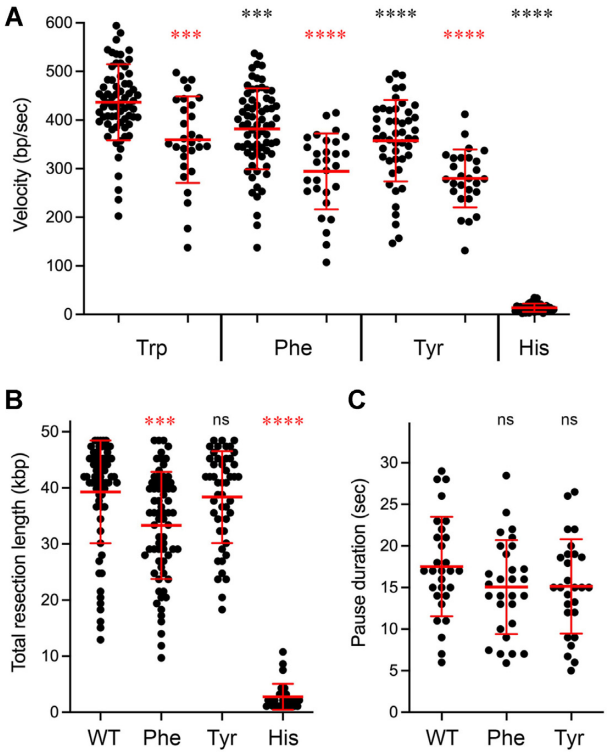

Figure 4. Summary of Trp325 mutational effects on single-molecule DNA resection. (**A**) Scatter plots of resection velocities during initial movement and after pausing. For each AdnAB protein specified below the x-axis, the initial movement velocities are plotted on the left and the after-pausing velocities are plotted on the right. Red lines indicate the mean ± SD. Black asterisks above each initial movement scatter plot summarize the *P* values of unpaired t tests of mutant versus wild-type initial movement velocities. Red asterisks above each after-pause scatter plot summarize the *P* values of unpaired t tests of after-pause versus initial movement for each AdnAB enzyme. (**B**) Resection tract length. Scatter plots of total DNA resection tract lengths. The observation period was 20 min for the His mutant; all other AdnAB proteins were observed for 5 min. Red lines indicate the mean ± SD. Red asterisks above each mutant scatter plot summarize the *P* values (unpaired t test of mutant versus wild-type). (**C**) Pause duration. Scatter plots of pause times between initial movement and resumption of resection. Red lines indicate the mean ± SD. *P* value symbols: ****, $P < 0.0001$; ***, $P < 0.001$; **, $P < 0.01$; *, $P < 0.05$; ns, not significant.

complex of AdnAB bearing a nuclease-inactivating mutation D934A of a metal-binding aspartate in the AdnA nuclease active site (10). Here, the wild-type AdnA subunit of the DNA-bound AdnA-AdnB(W325A)-DNA complex had a magnesium ion in the AdnA nuclease active site, situated adjacent to the terminal 5′ phosphate of the ssDNA tail, which had been cleaved two nucleotides away from the duplex junction (Supplementary Figure S4). The magnesium is in the vicinity of three putative metal-binding AdnA side chains: His833, Asp920, and Asp934 (Supplementary Figure S4). The backbone phosphates of the 5′ tail are contacted by AdnA residues Lys936, Lys939, and Ser940; Arg825 contacts the penultimate base of the cleaved 5′ strand (Supplementary Figure S4).

The salient insights from the DNA-bound AdnA-AdnB(W325A) structure concerned the fate of the flipped-out base of the 3′ ssDNA tracking strand and the impact of the W325A substitution on AdnB motif III. Anent the latter, it is important to note that the AdnB motif III peptide segment ^{323}YGWRGS^{328} is disordered in the cryo-EM structure of the DNA-free AdnAB apoenzyme yet becomes ordered when AdnAB binds to the forked duplex DNA (10). Here we found that this AdnB motif III peptide is disordered in the AdnA-AdnB(W325A)-DNA complex, signifying that the DNA-triggered conformational change in motif III depends on Trp325. As a result of the failure to elicit participation of the Ala325 mutant motif III peptide in the AdnB-DNA interface, the flipped-out **T** nucleobase adopts a continuously base-stacked arrangement (5′-$T^{-1}pT^{-2}p\mathbf{T}^{-3}pT^{-4}pG^{-5}$) with its flanking nucleotides. The structure model is depicted in Figure 5B, with bases numbered according to their positions relative to the duplex junction (as in Figure 1A and ref. 10). The Coulomb density maps for the DNA and amino acids are shown in Supplementary Figure S5A. A stereo view of the DNA map, oriented to highlight the continuous stacking of the T^{-2}, T^{-3}, T^{-4} and G^{-5} nucleobases, is shown in Supplementary Figure S5B. Comparison of the wild-type and W325A maps (Figs. S2 and S5A) affirms that the flipped-out T^{-3} base in the wild-type structure is instead stacked on the adjacent T^{-4} base in the W325A structure. The G^{-5} nucleobase remains stacked on the AdnB Phe254 phenyl ring in the W325A structure (Figure 5B and Supplementary Figure S5A), as seen in the wild-type AdnAB-DNA complex (Figure 1A and Supplementary Figure S2), and the insertion of Phe254 and Leu142 between the G^{-5} and T^{-6} bases recapitulates the discontinuity in base stacking of the distal tracking strand segment characteristic of the wild-type AdnAB-DNA complex. The phosphates of the 3′ tracking strand are contacted by AdnB residues Thr118, Arg81, Thr663, and Asn438, while Arg436 and Arg746 contact the T^{-1} base (Figure 5B), as observed in previous AdnAB-DNA structures (10). Whereas in prior structures the His665 side chain contacted the nucleobase upstream (5′) of the flipped-out base, in the W325A mutant structure H665 instead contacts the T^{-3} base (Figure 5B).

DISCUSSION

Here, we interrogated the effects of conservation substitutions for AdnB motif III constituent Trp325, which is essential for chemomechanical coupling in AdnAB and which is implicated in a ratchet-and-pawl mechanism entailing DNA base-stacking by Trp325 and associated base flipping in the 3′ ssDNA tracking strand (11). π–π stacking interactions of DNA and RNA nucleobases with protein aromatic amino acids tryptophan, phenylalanine, tyrosine, and histidine are prevalent in nature, as surmised from surveying high-resolution structures of DNA-protein and RNA-protein complexes (24,25). We found that AdnAB mutant heterodimers in which Trp325 was replaced by phenylalanine, tyrosine, histidine, leucine, or alanine retained activity in ssDNA-dependent ATP hydrolysis, but evinced a gradient of effects on ATP-dependent DNA end-resection activity, as gauged by concordant results of ensemble and single-molecule assays. The velocities of resection by the Phe325 and Tyr325 mutants were 90% and 85%, respectively, of the wild-type AdnAB velocity. By contrast, the His325 mutant slowed resection rate to 3% of wild-type and the Leu325

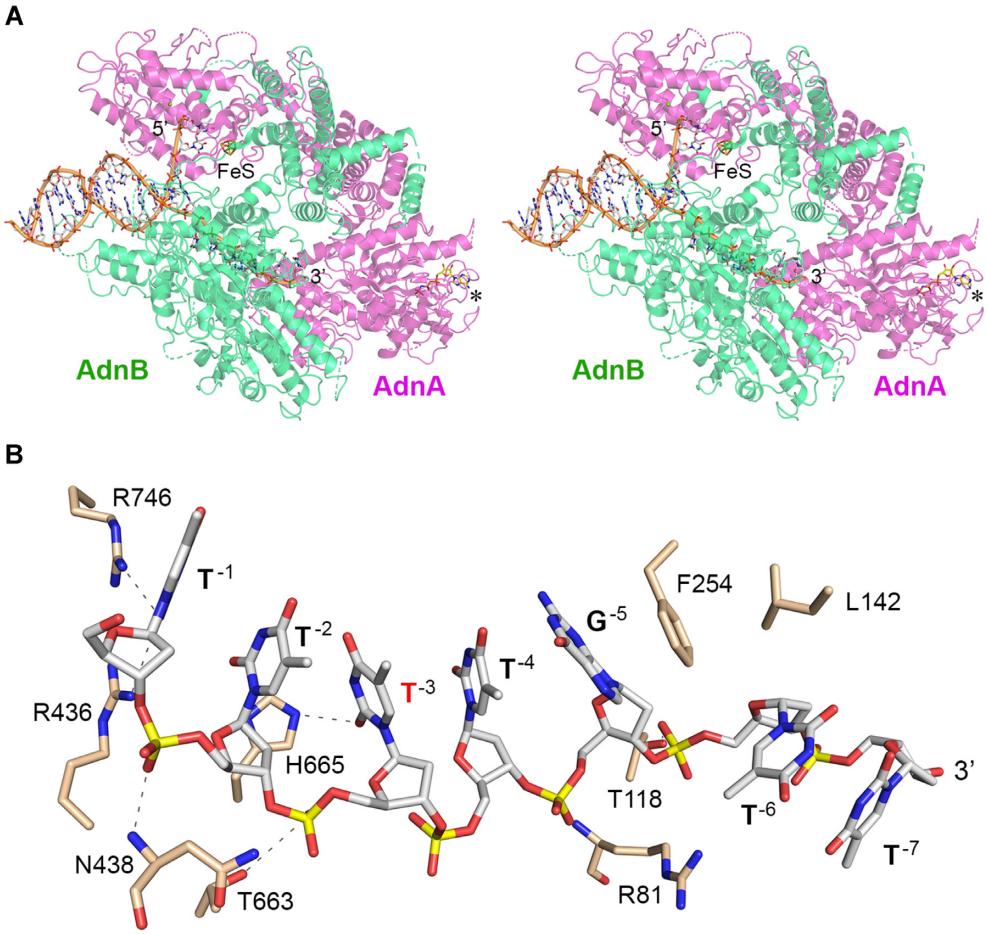

Figure 5. Cryo-EM structure of W325A mutant AdnAB in complex with tailed duplex DNA. (**A**) Stereo view of the AdnA-AdnB(W325A) heterodimer (semi-transparent cartoon model; magenta AdnA and green AdnB) in complex with forked duplex DNA (stick model with cartoon trace through the phosphodiester backbone). The 5′ and 3′ ssDNA ends are indicated. The iron-sulfur cluster (FeS) in the AdnA nuclease domain shown as a stick model. AMPPNP bound to the AdnA motor-like domain is depicted as a stick model with yellow carbons and denoted by an asterisk. (**B**) Interface of the 3′ ssDNA tracking strand with amino acids of the AdnB-(W325A) subunit. DNA is depicted as a stick model with gray carbons and yellow phosphorus atoms. The identities of the nucleobases are indicated in bold font and numbered by position relative to the duplex junction. Amino acids are rendered as stick models with beige carbons. The thymine (in red font) that was flipped out in the wild-type AdnAB-DNA complex (Figure 1A) is now in a continuous base stack on the flanking nucleobases.

variant was completely defective in DNA resection *à la* the Ala325 mutant.

The structure-activity-relations at Trp325 indicate that an aromatic side chain with a ring of 6 or more atoms is necessary for effective chemomechanical coupling of ATP hydrolysis to helicase translocation through dsDNA and ensuing DNA resection. We infer that this requirement for aromaticity comes into play as Trp325 engages in a π-stacking interaction with a tracking strand nucleobase adjacent to (5′ of) a flipped-out nucleobase observed in cryo-EM analyses of DNA-bound AdnAB. The modest superiority of Trp325 versus Phe325 and Tyr325 with respect to velocity of resection (and hence helicase movement) might reflect the larger π system of the 9-member indole ring versus a 6-member phenyl ring. Histidine proved to be inadequate as a replacement for Trp325, notwithstanding that its imidazole ring is similar in structure and aromaticity to the 5-membered component ring of indole. It is possible that protonation of the histidine to confer positive charge, or formation of hydrogen bond interactions to His-Nδ (not present in tryptophan) interfere with formation/stability of a proper π interaction with the tracking strand DNA base.

To better understand how the loss of Trp325 decouples the AdnB motor from ATP hydrolysis, we attained a cryo-EM structure of the W325A AdnAB mutant bound to a forked duplex DNA that had undergone incision of the 5′ ssDNA tail within the AdnA nuclease active site. The instructive differences between this structure and that of wild-type AdnAB on the same DNA (10) were that the absence of Trp325 prevented a DNA-triggered structural transition in AdnB motif III, whereby the ^{323}YGWRGAS^{329} motif III peptide that is disordered in the apoenzyme (i.e. no interpretable Coulomb potential in the cryo-EM map) becomes ordered upon interaction with the 3′ ssDNA tracking strand. In the DNA-bound AdnA–AdnB(W325A) structure, the 7-nucleotide 3′ tracking strand tail follows a similar trajectory through the AdnAB motor domain as in the wild-type complex and is engaged by a series of contacts with

AdnB side chains, as the wild-type complex, with the exception of the contacts made by motif III, i.e., because the motif III peptide ^{325}ARGASA^{330} is disordered in the AdnA–AdnB(W325A)–DNA complex. As a result, we did not observe in the W325A mutant structure the cation–π stacking of Arg326 on the T^{-4} base that was seen in the wild-type complex (Figure 1A). Note that the total chemomechanical decoupling phenotype of the W325A mutant cannot be attributed to lack of the Arg326 DNA contact, insofar as an AdnA-AdnB(R326A) mutant enzyme retained vigorous DNA resection activity at 80% of the velocity of wild-type AdnAB (11). Rather, the key finding here is that absent Trp325 and assimilation of motif III into the AdnB–DNA interface, the erstwhile flipped out T^{-3} nucleobase forms a continuous base-stacked array with its neighbors (Supplementary Figure S5B). We conclude that π stacking of motif III Trp325 on a ssDNA nucleobase triggers and stabilizes the flipped-out conformation of the neighboring nucleoside that underlies the creation of a ratchet pawl.

The present findings prompt us to speculate that the conformational flexibility of the AdnB motif III peptide might come into play during ATP-driven translocation of the motor on the tracking strand. The ATPase cycle of SF1 helicases entails oscillating movements of the RecA-like domains of the motor subunit (26,27). Previous mutational analyses of the AdnB motor implicated residues Thr118, Thr663, and His665 and their contacts to the tracking strand as important for chemomechanical coupling, i.e., their replacement individually by alanine drastically reduced DNA resection velocity *vis-à-vis* wild-type AdnAB (11). We suggested that their contacts couple the output of the ATP hydrolysis cycle to forward movement of the DNA strand through the AdnB motor domain during the power stroke of ATP hydrolysis, after which they are reset, and offset, by a one-nucleotide interval of the tracking strand. Because the Trp325 nucleobase stack would appear to be an impediment to forward slippage of the tracking strand, it must either be the case that: (i) the stacked base (T^{-2} in Figure 1A) slides around a stationary Trp325 and into the flipped-out state of the previous T^{-3} base; or (ii) Trp325 (and perhaps together with Arg326) transiently moves out of the way to allow DNA translocation, after which it re-engages to stack on the translocated T^{-1} base and drive flipping out of the T^{-2} base. The latter model fits with the seemingly dynamic state of motif III in the available cryo-EM structures of AdnAB.

DATA AVAILABILITY

The atomic structure model of the AdnA-AdnB(W325A)•DNA complex has been deposited in the PBD and EMDB databases under ID codes 7SJR and EMD-25164, respectively.

SUPPLEMENTARY DATA

Supplementary Data are available at NAR Online.

FUNDING

NIH [R35-GM126945, R01-AI64693 to S.S., R01-CA236606 to E.C.G.]; D.J.P. is supported by the Maloris Foundation; the Memorial Sloan-Kettering Structural Biology Core Facility is supported by National Cancer Institute [P30-CA008748]; the funders had no role in study design, data collection and analysis, decision to publish or preparation of the manuscript. Funding for open access charge: NIH [R01-AI64693].
Conflict of interest statement. None declared.

REFERENCES

1. Sinha,K.M., Unciuleac,M.C., Glickman,M.S. and Shuman,S. (2009) AdnAB: a new DSB-resecting motor-nuclease from mycobacteria. *Genes Dev.*, **23**, 1423–1437.
2. Gupta,R., Barkan,D., Redelman-Sidi,G., Shuman,S. and Glickman,MS. (2011) Mycobacteria exploit three genetically distinct DNA double-strand break repair pathways. *Mol. Microbiol.*, **79**, 316–330.
3. Wigley,D.B. (2013) Bacterial DNA repair: recent insights into the mechanism of RecBCD, AddAB and AdnAB. *Nat. Rev. Microbiol.*, **11**, 9–13.
4. Rand,L., Hinds,J., Springer,B., Sander,P., Buxton,R.S. and Davis,E.O. (2003) The majority of inducible DNA repair genes in *mycobacteriumtuberculosis* are induced independently of recA. *Mol. Microbiol.*, **50**, 1031–1042.
5. Namouchi,A., Gómez-Muñoz,M., Frye,S.A., Moen,L.V., Rognes,T., Tønjum,T. and Balasingham,S.V. (2016) The *mycobacteriumtuberculosis* transcriptional landscape under genotoxic stress. *BMC Genomics*, **17**, 791.
6. Müller,A.U., Imkamp,F. and Weber-Ban,E. (2018) The mycobacterial lexa/reca-independent DNA damage response is controlled by PafBC and the Pup-proteasome system. *Cell Rep.*, **23**, 3551–3564.
7. Unciuleac,M.C. and Shuman,S. (2010) Characterization of the mycobacterial AdnAB DNA motor provides insights into the evolution of bacterial motor-nuclease machines. *J. Biol. Chem.*, **285**, 2632–2641.
8. Unciuleac,M.C. and Shuman,S. (2010) Double strand break unwinding and resection by the mycobacterial helicase-nuclease AdnAB in the presence of single-strand DNA-binding protein (SSB). *J. Biol. Chem.*, **285**, 34319–34329.
9. Gupta,R., Unciuleac,M.C., Shuman,S. and Glickman,M.S. (2017) Homologous recombination mediated by the mycobacterial AdnAB helicase without end resection by the AdnAB nucleases. *Nucleic Acids Res.*, **45**, 762–774.
10. Jia,N., Unciuleac,M.C., Xue,C., Greene,E.C., Patel,D.J. and Shuman,S. (2019) Structures and single-molecule analysis of bacterial motor nuclease AdnAB illuminate the mechanism of DNA double-strand break resection. *Proc. Natl. Acad. Sci. U.S.A.*, **116**, 24507–24516.
11. Unciuleac,M.C., Meir,A., Xue,C., Warren,G.M., Greene,E.C. and Shuman,S. (2021) Clutch mechanism of chemomechanical coupling in a DNA resecting motor-nuclease. *Proc. Natl. Acad. Sci. U.S.A.*, **118**, e2023955118.
12. De Tullio,L., Kaniecki,K. and Greene,E.C. (2018) Single-stranded DNA curtains for studying the srs2 helicase using total internal reflection fluorescence microscopy. *Methods Enzymol.*, **600**, 407–437.
13. Xue,C., Wang,W., Crickard,B., Moevus,C., Kwon,Y., Sung,P. and Greene,E.C. (2019) Regulatory control of sgs1 and dna2 during eukaryotic DNA end resection. *Proc. Natl. Acad. Sci. U.S.A.*, **116**, 6091–6100.
14. Zheng,S.Q., Palovcak,E., Armache,J.P., Verba,K.A., Cheng,Y. and Agard,D.A. (2017) MotionCor2: anisotropic correction of beam-induced motion for improved cryo-electron microscopy. *Nat. Methods*, **14**, 331–332.
15. Rohou,A. and Grigorieff,N. (2015) CTFFIND4: fast and accurate defocus estimation from electron micrographs. *J. Struct. Biol.*, **192**, 216–221.
16. Zivanov,J., Nakane,T., Forsberg,B.O., Kimanius,D., Hagen,W.J., Lindahl,E. and Scheres,S.H. (2018) New tools for automated high-resolution cryo-EM structure determination in RELION-3. *Elife*, **7**, e42166.

17. Scheres,S.H. and Chen,S. (2012) Prevention of overfitting in cryo-EM structure determination. *Nat. Methods*, **9**, 853–854.
18. Pettersen,E.F., Goddard,T.D., Huang,C.C., Couch,G.S., Greenblatt,D.M., Meng,E.C. and Ferrin,TE. (2004) UCSF Chimera–a visualization system for exploratory research and analysis. *J. Comput. Chem.*, **25**, 1605–1612.
19. Goddard,T.D., Huang,C.C., Meng,E.C., Pettersen,E.F., Couch,G.S., Morris,J.H. and Ferrin,T.E. (2018) UCSF chimerax: meeting modern challenges in visualization and analysis. *Protein Sci.*, **27**, 14–25.
20. Emsley,P., Lohkamp,B., Scott,W.G. and Cowtan,K. (2010) Features and development of coot. *Acta. Crystallogr.*, **D66**, 486–501.
21. Adams,P.D., Afonine,P.V., Bunkóczi,G., Chen,V.B., Davis,I.W., Echols,N., Headd,J.J., Hung,L., Kapral,G.J., Grosse-Kunstleve,R.W. *et al.* (2010) PHENIX: a comprehensive Python-based system for macromolecular structure solution. *Acta Crystallogr.*, **D66**, 213–221.
22. Collins,B.E., Ye,L.F., Duzdevich,D. and Greene,E.C. (2014) DNA curtains: novel tools for imaging protein–nucleic acid interactions at the single-molecule level. *Methods Cell Biol.*, **123**, 217–234.
23. Finkelstein,I.J., Visnapuu,M.L. and Greene,E.C. (2010) Single-molecule imaging reveals mechanisms of protein disruption by a DNA translocase. *Nature*, **468**, 983–987.
24. Wilson,K.A., Kellie,J.L. and Wetmore,S.D. (2014) DNA–protein π-interactions in nature: abundance, structure, composition and strength of contacts between aromatic amino acids and DNA nucleobases or deoxyribose sugar. *Nucleic Acids Res.*, **42**, 6726–6741.
25. Wilson,K.A., Kung,R.W., D'souza,S. and Wetmore,S.D. (2021) Anatomy of noncovalent interactions between the nucleobases or ribose and π-containing amino acids in RNA–protein complexes. *Nucleic Acids Res.*, **49**, 2213–2225.
26. Yang,W. (2010) Lessons learned from UvrD helicase: mechanism for directional movement. *Annu. Rev. Biophys.*, **39**, 367–385.
27. Lee,J.Y. and Yang,W. (2006) UvrD helicase unwinds DNA one base pair at a time by a two-part power stroke. *Cell*, **127**, 1349–1360.